IEEE Access
Multidisciplinary | Rapid Review | Open Access Journal

Received December 9, 2020, accepted December 31, 2020, date of publication January 18, 2021, date of current version February 2, 2021.

Digital Object Identifier 10.1109/ACCESS.2021.3052687

Pade-Approximation Based Behavioral Modeling for RF Power Amplifier Design

CIARÁN WILSON[1], (Member, IEEE), ANDING ZHU[1], (Senior Member, IEEE), JIALIN CAI[2], (Senior Member, IEEE), AND JUSTIN B. KING[3], (Senior Member, IEEE)

[1]School of Electrical and Electronic Engineering, University College Dublin, Dublin 4, D04 V1W8 Ireland
[2]Key Laboratory of RF Circuit and System, Ministry of Education, Hangzhou Dianzi University, Hangzhou 310018, China
[3]Department of Electronic and Electrical Engineering, Trinity College Dublin, Dublin 2, D02 PN40 Ireland

Corresponding author: Ciarán Wilson (ciaran.wilson@ucdconnect.ie)

This work was supported by the Science Foundation Ireland under Grant 13/RC/2077.

ABSTRACT Radio frequency (RF) power amplifier (PA) design using Gallium Nitride (GaN) transistor technology requires accurate device models in order to maximise performance and reduce development time. The current state-of-the-art frequency-domain behavioural models focus on linear and quadratic approximations to the polyharmonic distortion (PHD) formalism. However, the linear approximation suffers from poor accuracy under load mismatch conditions, while the quadratic approximation suffers from poor extrapolation beyond the measured range, leading to erroneous predictions of the optimum load impedances for maximum output power and maximum drain efficiency. In this work, a rational Padé-based approximation is proposed as the model core, and it is shown, through experimental validation, that the Padé approximation-based model can provide superior results in a more scalable format. It can mitigate problems found in the existing PHD models when applied to the matching problem. Specifically, the proposed model produces fewer erroneous solutions for the optimum load points, due to the well-behaved nature of Padé approximants. In addition, for the first time, results are reported on using the behavioural model to determine the optimum impedance for maximum transducer gain in a two-port device model. All results show the Padé model has high potential when compared to the established PHD-derived models in RF PA design.

INDEX TERMS Behavioural modelling, Padé approximation, polyharmonic distortion (PHD) modelling, X-parameter model.

I. INTRODUCTION

The cellular communication industry is a significant consumer market in the world today, with GSMA Intelligence estimating that the number of unique mobile subscribers worldwide is over 5 billion [1]. With the roll-out of the fifth generation (5G) mobile communication networks across the world, data rates for mobile devices have increased dramatically. This poses huge challenges for power amplifier (PA) designers in maintaining high efficiency across broad bandwidths, as well as extracting maximum performance from the active device. For this type of radio frequency (RF) design, an accurate and robust device model is seen as essential to deliver the required level of performance.

Gallium Nitride (GaN) is often regarded as the most promising semiconductor technology for these applications that require simultaneous operation at high frequency and high power [2]. GaN devices are able to achieve an order of magnitude improvement in power density when compared to other traditional compound semiconductors, such as gallium arsenide (GaAs). A key enabler of this is the high breakdown electric field ($E_{br} \approx 4$ MV/cm) inherent in this technology due to the large bandgap ($E_g \approx 3.4$eV) [3]. This allows for a larger voltage swing across the device output terminals compared to traditional technologies, such as metal oxide semiconductor (MOS) technology. This large voltage swing is useful for designing certain classes of highly efficient PAs, such as the popular continuous class-F PA which exhibit voltage peaks well above 150% of the drain supply voltage value [4].

Within the device modelling research field, there are three distinct types of models: physical, equivalent circuit and behavioural models. This research is focused on behavioural models. Behavioural models have been shown to be very

The associate editor coordinating the review of this manuscript and approving it for publication was Vittorio Camarchia.

effective at describing the RF frequency domain behaviour of GaN-based transistor devices [5]. The popularity of the behavioural approach is two-fold. Firstly, behavioural models, sometimes referred to as ''black-box'' models, require no knowledge of the inner workings of the device, resulting in fast model extraction. This differs markedly from the two other competing modelling paradigms, namely: physical models and equivalent circuit models [6], [7]. Secondly, since such models are built directly from measurement data, they are typically very accurate in the operating region from which they have been extracted.

The scattering parameter (S-parameter) formalism is an example of arguably the most successful frequency-domain behavioural model. However, S-parameters are only valid for linear, time-invariant systems (or systems that can be approximated as such), and cannot model devices with nonlinear behaviour [8], [9].

The PHD (polyharmonic distortion) models, introduced in [10], are designed to extend the scattering parameter approach to the nonlinear domain i.e. PHD models can be applied to nonlinear time-invariant devices or systems. Given the significantly more complex behaviour of devices in the nonlinear regime, an approximation of the PHD model is generally used, such as the first order Taylor series approximation, known as X-parameters. Higher order approximations are also possible, e.g. the quadratic PHD (QPHD) model [11], [12]. As the order increases, such polynomial based models can approach global accuracy i.e. maintain accurate prediction across the full Smith chart under moderate-to-high mismatch conditions. However, higher order polynomials do not extrapolate well, can result in overfitting, and can be difficult to extract [12].

Padé approximations, on the other hand, are based on rational functions (a quotient of polynomial functions). This ensures the model is better behaved, particularly when evaluated beyond the modelled range i.e. during extrapolation. This is due to the superior convergence typically observed for Padé approximants compared to that of a Taylor series [13], where Padé approximants can even yield acceptable results around points for which a Taylor series diverges.

This paper is structured as follows. In Section II, a brief overview of the Padé model approximation applied to the PHD formalism is provided, along with a statement of the large-signal matching problem and its solution, this represents the first time the Padé model has been used to solve the large-signal matching problem. In Section III, a Padé model is extracted from a GaN transistor device, and used to determine directly from the model, the load impedances corresponding to maximum output power and maximum efficiency. These predicted results from the model are then compared with corresponding loadpull measurement data as well as being compared with other state-of-the-art models. In Section IV, the investigation of a load-dependent Padé model is carried out, with results and discussion provided. The proposed model is also extended to determine the conditions for maximum transducer gain from a two-port device for the first time.

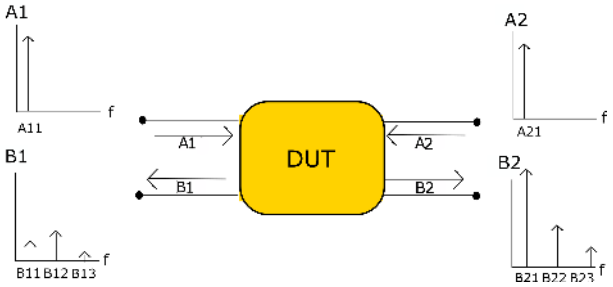

FIGURE 1. Types of scattered waves needed for a model extraction of a given DUT.

II. THEORY OF LARGE-SIGNAL MATCHING USING BEHAVIOURAL SCATTERING WAVE MODELS

Consider the device under test (DUT) shown in Fig. 1. The incident and scattered waves are indicated at port-1 as A_1 and B_1, respectively, and those at port-2 are indicated as A_2 and B_2. These waves may be further broken down into their constituent harmonics e.g. A_{12} for the second harmonic in the incident wave at port-1. These *pseudowaves* are linear combinations of the complex port voltage amplitude V_{ph} and complex port current amplitude I_{ph}, as shown in (1a), where the current is defined as positive when flowing into the port, p is the port number, and h is the harmonic index

$$A_{qn} = \frac{V_{qn} + Z_0 I_{qn}}{2\sqrt{Z_0}} \tag{1a}$$

$$B_{ik} = \frac{V_{ik} - Z_0 I_{ik}}{2\sqrt{Z_0}}, \tag{1b}$$

where, for simplicity, it is assumed that Z_0 is purely real.

In order to describe the DUT in the frequency domain, we need some way to relate the incident and scattered waves. In principle, a describing function F could provide the nonlinear spectral mapping required for an extension of the scattering formalism to this nonlinear domain, as shown in (2) below,

$$B_{ik} = F_{ik}(A_{11}, A_{12}, \ldots, A_{21}, A_{22}, \ldots,), \tag{2}$$

which relates the complex amplitude A_{qn} of the incident waves at device port q and harmonic index n to the complex amplitude B_{ik} of the scattered waves, at device port i and harmonic index k. Separate functions F_{ik} are required for each port i and harmonic index k for which the value of the amplitude and phase of the scattered wave are desired. Such a modelling framework, known as the poly-harmonic distortion (PHD) model, has been introduced by Verspecht and Root [10]. However, describing functions such as these, which must account for all A-waves at every port and at every harmonic, would require a prohibitively large data-set and elaborate set of functions F_{ik}. To solve this problem, Verspecht and Root proposed a linearisation of the PHD model, known as X-parameters [14]. In the original form of X-parameters, a single incident wave at a single harmonic (usually the fundamental input wave) is treated as the dominant tone, and all others are considered as linear perturbations.

A basic X-parameter model is implemented by (3), giving B_{21} i.e. the scattered wave at port-2, in terms of the X-parameters (which depend on the dominant wave A_{11}), A_{21} i.e. the small-signal perturbation in the fundamental at port-2, and its conjugate, A_{21}^*,

$$B_{21} = X_{21}^F + X_{21,21}^S A_{21} + X_{21,21}^T A_{21}^*, \tag{3}$$

where it is assumed, here, for simplicity, that A_{11} has zero phase. The quantity X_{ik}^F accounts for the large-signal output wave due specifically to the large-signal input A_{11} at port-1, while $X_{21,21}^S$ and $X_{21,21}^T$ describe the contribution to B_{21} from the perturbation A_{21}. The need for two parameters ($X_{21,21}^S$ and $X_{21,21}^T$) to describe the effect of the small-signal perturbation is due to the nonholomorphic nature of the describing function mapping, F_{21} in this case. Previous attempts, such as Hot S-parameters, omitted the conjugate term and hence suffered from a fundamentally incorrect model structure. In general, the X-parameters are also functions of the dc bias and fundamental frequency [15].

The X-parameter model described above is reasonably accurate when the load impedance is matched, or nearly so, such that only a small wave is reflected back into the device. However, in highly mismatched systems this model can yield poor results. Load-dependent X-parameter [16] descriptions give improved results under load impedances far from the matched condition [17], as is often the case in PA designs. Load-dependent X-parameters means the X-parameters become, effectively, functions of the fundamental incident wave at port-2, A_{21} in addition to A_{11}. However, since A_{21} results from the scattered wave B_{21} reflecting back into the DUT due to the load mismatch, it is not possible to know this value *apriori*, and typically the X-parameters are given as functions of A_{11} and Γ_L, e.g. $X_{ik}^F(A_{11}, \Gamma_L)$, since Γ_L can be controlled during extraction. This grid structure facilitates tabulation of the X-parameters across a range of reflection coefficients over the Smith chart, which can be read and interpreted by a circuit simulator.

There is, however, a drawback to this improved accuracy: as mentioned, load-dependent X-parameters require tabulation of the parameter values versus Γ_L. This adds yet another dimension to the data. Effectively, each table entry describes a local model, valid around the vicinity of the Γ_L from which it is extracted. One way of mitigating this issue is to return to the standard X-parameter model in (3). We see it is effectively a first-order two dimensional Taylor series approximation to the describing function F_{ik}. Previous work has shown that this linear polynomial can be modified to include higher order terms e.g. a quadratic model [12]. Such models allow for larger perturbations at the load while maintaining a reasonable level of accuracy. However, some numerical difficulties arise even for this second degree case, and hence further attempts at improving the model fidelity via cubic, or higher order, polynomials, is likely to face more extreme versions of the same problem.

In this work, we build on previous modelling efforts [18]–[20] using Padé approximants, rather than polynomials, for simplification of the describing functions F_{ik}. For the first time, we show the Padé-based model can provide significant advantages compared with the state-of-the-art when solving, numerically, the large-signal matching problem. We demonstrate how the Padé model enables a more accurate prediction of the optimum load impedance for a given criterion, i.e. the impedance that maximises the desired metric (power delivered, drain efficiency or operating gain). The rational nature of the approximation allows higher order models to be considered when it is necessary to model, accurately, complex device behaviour. This is, in general, not possible using poorly-behaved polynomial functions.

A. PADÉ APPROXIMATION THEORY AND EXTRACTION

A 1-D Padé approximant is defined as

$$R_1(x) = \frac{P_1(x)}{Q_1(x)} = \frac{\sum_{r=0}^{N} G_r x^r}{1 + \sum_{r=1}^{M} H_r x^r}, \tag{4}$$

where G and H are the coefficients for the numerator and denominator respectively, x is the independent variable, and the order of the Padé approximant is indicated using the notation $[N/M]$.

However, as discussed in the introduction to this section, PHD-based models require a 2-D approximation, since we must consider the perturbation and its conjugate as distinct independent variables. Extending (4) to a 2-D rational approximation [13], gives

$$R_2(x, y) = \frac{P_2(x, y)}{Q_2(x, y)} = \frac{\sum_{(r,s)=0}^{N,N'} G_{rs} x^r y^s}{1 + \sum_{(r,s)\neq(0,0)}^{M,M'} H_{rs} x^r y^s}, \tag{5}$$

which represents a 2-D Padé approximation, sometimes known as a *Chisholm* approximant [21]. We can write the order as $[NN'/MM']$.

If we approximate an expression $f(x, y)$ around the steady-state point (X, Y), based on (5), we get

$$\begin{aligned} f(X + \Delta x, Y + \Delta y) &\approx R_2(X + \Delta x, Y + \Delta y) \\ &= \frac{P_2(X + \Delta x, Y + \Delta y)}{Q_2(X + \Delta x, Y + \Delta y)} \\ &= \frac{\sum_{(r,s)=0}^{N,N'} G_{rs}(X, Y) \Delta x^r \Delta y^s}{1 + \sum_{(r,s)\neq(0,0)}^{M,M'} H_{rs}(X, Y) \Delta x^r \Delta y^s}, \end{aligned} \tag{6}$$

where Δx and Δy are small deviations caused by a small perturbation signal.

Applying it to the PHD model allows us to make the following equivalences

$$\begin{aligned} (X, Y) &\equiv (|A_{11}|) \\ \Delta x &\equiv A_{qn} \\ \Delta y &\equiv (A_{qn})^* \end{aligned} \tag{7}$$

For an expression $f(x, y)$ around the steady state point (X, Y). Where q and n are the port and harmonic respectively. If we

say $N = 1, N' = 1, M = 1$ and $M' = 1$ then we end up with notation for a Padé 11/11 model, to use the notation in [18].

If we say that the scattered wave B_{pm} is written as

$$B_{ik} = F'_{ik}(|A_{11}|, A_{qn}, (A_{qn})^*) \tag{8}$$

where F'_{ik} is a (new) describing function that associates all of the relevant incident waves A_{qn} with the scattered waves B_{pm}. Then after using the harmonic superposition principle and the 2-D Padé approximation method (8) can be represented as

$$B_{ik} = \frac{G_{ik,00} + \sum_{qn} \sum_{(r,s)=0}^{N,N'} G_{ik,qn,rs}(A_{qn})^r [A^*_{qn}]^s}{1 + \sum_{qn} \sum_{(r,s)\neq 0}^{M,M'} H_{ik,qn,rs}(A_{qn})^r [A^*_{qn}]^s} \tag{9}$$

Note that for this work i and q will be equal to 2 and k and n equal to 1, therefore the notation of the coefficients can be shortened for simplicity as will be shown later. This is done for the same reasons as in [12], to limit the model the model size and because linear PHD terms allow for sufficient accuracy even when allowing for harmonic mismatch.

B. FORMULATION OF THE LARGE-SIGNAL MATCHING PROBLEM VIA LINEAR AND QUADRATIC APPROXIMANTS

In linear circuits, maximum power transfer from a source to a load is facilitated by a load impedance equal to the complex conjugate of the source impedance. In the case of a nonlinear transistor, however, no such general analytical method exists. However, in the recent literature it is shown how an equation may be formulated using an X-parameter model, and solved, analytically, to identify the optimum load that maximises the output power [22]. The formulation of this problem begins by examining the net output power at port-2 of the DUT, as given by (10)

$$P_{\text{OUT}} = \frac{|B_{21}|^2 - |A_{21}|^2}{2}, \tag{10}$$

where $|B_{21}|^2/2$ represents the power in the wave emanating from port-2 of the DUT, while $|A_{21}|^2/2$ represents the power in the wave that is incident back into port-2 of the DUT. This output power is maximised at the values of A_{21} where (10) is stationary, i.e. it is required to solve

$$\frac{\partial P_{\text{OUT}}}{\partial A_{21}} = \frac{\partial(|B_{21}|^2 - |A_{21}|^2)}{\partial A_{21}} \tag{11}$$

The variable B_{21} can be eliminated using the X-parameter model, e.g. (3), and the resulting optimisation problem in the single variable A_{21} may by solved to obtain the reflection coefficient A_{21}/B_{21} of the optimum load for maximum output power.

While not a general method (since it only solves an approximated problem via the X-parameter model), in practice it yields reasonable results. An extension of this method for use with quadratic PHD (QPHD) models is given in [12]. However, in this case, a closed-form analytical solution is not possible, hence the optimisation problem in (11) is solved numerically.

When using the QPHD model for B_{21}, it is typical that multiple solutions to (11) exist [12]. In reality, there generally exists only a single optimum load impedance for maximum output power. Some of the solutions to (11) correspond to points outside the Smith chart, and can therefore be neglected outright (as they cannot be realised with a passive load). Other erroneous solutions also arise; these are due to poor QPHD model extrapolation. This will be discussed again shortly.

C. FORMULATION OF THE LARGE-SIGNAL MATCHING PROBLEM VIA PADÉ APPROXIMANT

As an alternative to polynomial-based models, *Padé* approximants have also been applied to frequency-domain behavioural modelling problems, with positive results [18]. The mathematical background of the Padé approximant has been discussed in detail in Section II-A. It is evident from the defining equation (5), that when the numerator and denominator polynomials have equal order the Padé model will be bounded – it is important to be aware that this property is not possible from a polynomial-based model.

For demonstrative purposes, we proceed with the simple example of the Padé [11/11] model to use the notation from [18], where $[NN'/MM']$ implies an N-th order expansion in A_{21} and a P-th order expansion in A^*_{21} in the numerator, with MQ providing the same information for the denominator. This means that the Padé [11/11] shown in (12) below only has one more coefficient than the QPHD model

$$B_{21} = G_{21} + \frac{G_{21,10}A_{21} + G_{21,01}A^*_{21} + G_{21,11}A_{21}A^*_{21}}{1 + H_{21,10}A_{21} + H_{21,01}A^*_{21} + H_{21,11}A_{21}A^*_{21}} \tag{12}$$

where G_{21} plays the same role as X^{F}_{21} from (3) i.e. the represents the large-signal operating point (LSOP).

Returning to the matching problem, the Padé model can now be used to replaced the B_{21} variable in (11), giving

$$\frac{\partial}{\partial A_{21}}\left(\left|G_{21} + \frac{G_{21,10}A_{21} + G_{21,01}A^*_{21} + G_{21,11}A_{21}A^*_{21}}{1 + H_{21,10}A_{21} + H_{21,01}A^*_{21} + H_{21,11}A_{21}A^*_{21}}\right|^2 - |A_{21}|^2\right) = 0. \tag{13}$$

Similarly to the QPHD model, a simple analytical formulation is not possible for finding the optimum load in this case. Instead, a numerical solution can be obtained via standard solvers. Note that in all optimisation equations provided in this paper, the variables A_{21} and A^*_{21} are considered to be independent. To solve the resulting systems of one equation and two unknown values, the derivative with respect to the conjugate must also be used – see [22] for the details.

D. PADÉ MODEL EXTRACTION

To determine the coefficients for this model, i.e. to extract the model, we use the small range of measured sample points shown in Fig. 2. The selected load points are shown here at the 50 Ω load point and at 12 different phases at two different

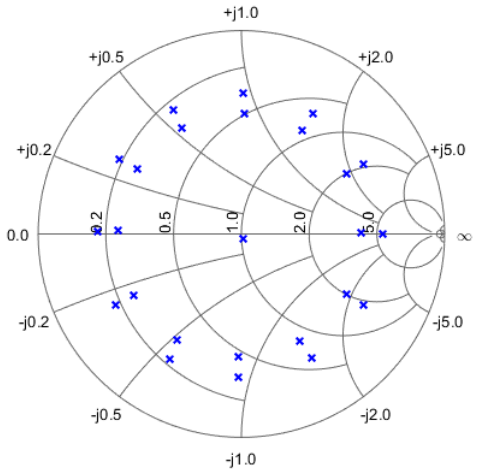

FIGURE 2. Sample of load-points taken for model extraction.

magnitudes of Γ, therefore there are exactly 25 unique data points used for model extraction. Theoretically 12 unique phase points would be enough to extract a Padé model with 12 independent coefficients. However, in order to keep the comparison with the QPHD model fair the number of coefficients should be similar in size to the full QPHD model which is six coefficients. Generally it is best practice to take more measurements than theoretically needed in order to minimise the effects of noise. It is possible that more data points than the 25 used for this extraction will make the models more robust to noise, however it was found that 25 points extracted macro models with good accuracy.

After the sample points are taken, we can get the matrix formulation of the problem. In this case the problem is how to extract a Padé [11/11] model, as shown in

$$P_A = \begin{bmatrix} 1 & A_{21,1} & A^*_{21,1} & A_{21,1}A^*_{21,1} \\ 1 & A_{21,2} & A^*_{21,2} & A_{21,2}A^*_{21,2} \\ \vdots & \vdots & \vdots & \vdots \\ 1 & A_{21,n} & A^*_{21,n} & A_{21,n}A^*_{21,n} \end{bmatrix} \tag{14}$$

$$P_{AB} = \begin{bmatrix} -B_{21,1}A_{21,1} & -B_{21,1}A^*_{21,1} & -B_{21,1}A_{21,1}A^*_{21,1} \\ -B_{21,2}A_{21,2} & -B_{21,2}A^*_{21,2} & -B_{21,2}A_{21,2}A^*_{21,2} \\ \vdots & \vdots & \vdots \\ -B_{21,n}A_{21,n} & -B_{21,n}A^*_{21,n} & -B_{21,n}A_{21,n}A^*_{21,n} \end{bmatrix}$$

$$\begin{bmatrix} B_{21,1} \\ B_{21,2} \\ \vdots \\ B_{21,n} \end{bmatrix} = \begin{bmatrix} P_A & P_{AB} \end{bmatrix} \begin{bmatrix} G_{21} \\ G_{21,10} \\ G_{21,01} \\ G_{21,11} \\ H_{21,10} \\ H_{21,01} \\ H_{21,11} \end{bmatrix} \tag{15}$$

This matrix formulation can be presented symbolically as

$$\mathbf{B} = \mathbf{AC}_o \tag{16}$$

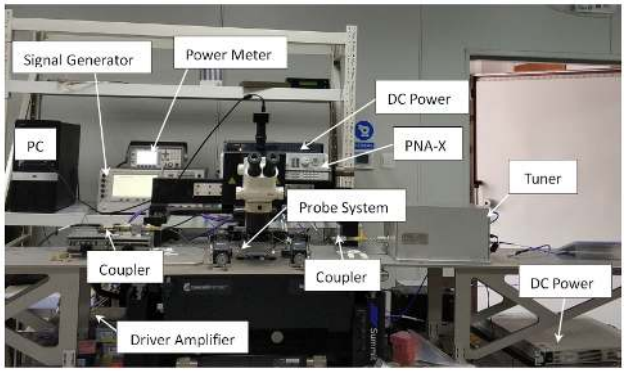

FIGURE 3. Loadpull setup for extracting Padé model.

Because **A** is complex and not always square, we have to obtain the pseudo-inverse

$$\mathbf{A}^H\mathbf{B} = \mathbf{A}^H\mathbf{AC_o} \tag{17}$$

Matrices denoted with a "H" superscript are the Hermetian conjugate of that matrix. Now, the model coefficients can be obtained according to

$$\mathbf{C}_o = (\mathbf{A}^H\mathbf{A})^{-1}\mathbf{A}^H\mathbf{B} \tag{18}$$

III. MEASUREMENT RESULTS USING PADÉ-BASED MODEL

In order to investigate the real world efficacy of the proposed Padé-based modelling technique, loadpull-based waveform data is experimentally obtained from a 10W GaN device manufactured by CREE, CGH40010F. The transistor is measured at a class-AB bias point, with V_{GS} equal to −3 V and V_{DS} equal to 28 V.

The A_{11} input tone is injected at the DUT input using a driver amplifier (where necessary), while an active load-pull system is used to synthesise an A_{21}-wave impinging on port-2 of the device. The particular experimental setup used to extract the data for this work is shown in Fig. 3. This effects a change in the load impedance implemented at the output of the DUT. Note that if the losses in the loadpull system tuner(s) are low (which they typically are at low frequencies), a passive loadpull system may suffice for model extraction.

Measurements are taken across a range of input powers: 10 dBm, 20 dBm and 30 dBm, with a fundamental frequency of 1.5 GHz. These measurements are carried out with a fixed source impedance of 50 Ω. Once the measurements are collected the model can be extracted in MATLAB, according to Section II-D.

A. MULTIPLE OPTIMA PROBLEM AND SOLUTION

A major advantage of the Padé model is that it tends to produce fewer erroneous load impedance values for a given metric of interest. In [12], it is stated that the QPHD model can produce 'false positive' results i.e. multiple values satisfying (11) can be returned, all but one of which are mathematical artifacts that do not correspond to a true optimum e.g. maximum output power. Due to the order of the polynomial

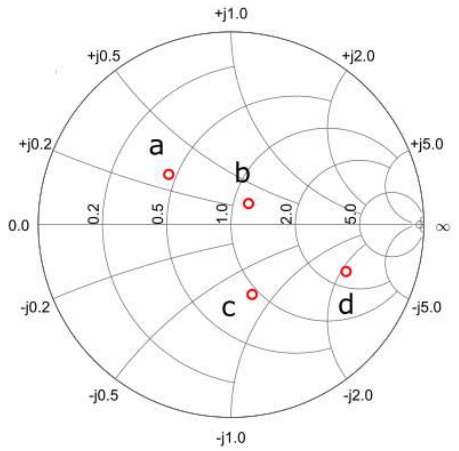

FIGURE 4. QPHD models multiple predictions for optimum loads represented on a Smith chart.

used for the QPHD model, there will be nine unique solutions to it. While some of these can be immediately dismissed, such as those outside the Smith chart, in this work it has been shown that many solutions are returned inside the Smith chart, in general, with no obvious method of eliminating the erroneous values. The exact number of such false positives returned depends on the measurement conditions, such as input power level, and the selection of loadpull data that is used for the least-squares model extraction.

For example, Fig. 4 shows four (potential) optimum load points for maximum output power, as predicted by a QPHD model extracted from loadpull data in the usual way, i.e., similar to the method given for Padé model extraction in Section II-D. This poses many problems as, without any prior information as to where the true optimum load point is (in general there will be only one), it is not obvious which one of these predicted optimum loads is correct, i.e., which one is closest to the optimum load for maximum power that would be determined via extensive brute-force loadpull measurement on the real device.

In this work, a simple and accurate way of eliminating these false positives is identified and will now be explained. Recall how each of the behavioural models discussed in this paper are based on predicting the scattered wave dependent variable, say B_{21}, for known values of the independent variable e.g. A_{11}, A_{21} etc. For optimum load prediction, however, the quantity of interest is the ratio of A_{21} to B_{21}, namely the load reflection coefficient $\Gamma_{\mathrm{L}} = A_{21}/B_{21}$. Hence, while sensible values for Γ_{L} may be returned (i.e. where $\Gamma_{\mathrm{L}} < 1$) as potential optimum loads via numerical solution of (11), it is possible that A_{21} and B_{21} themselves are well outside of the accurately modelled range.

The A_{21} values for the four optimum load points inside the Smith chart are shown in Table 1. Given that the measured values of the reflected wave at the load, A_{21}, extend between ± 0.65 W$^{1/2}$ on the real axis, and approximately the same for imaginary A_{21} axis, we can see that only one of the A_{21} values is within this measured range (the value labelled

TABLE 1. A_{21} values for $\Gamma_{opt,QPHD}$.

label	$\lvert A_{21}\rvert$	A_{21} values	$\Gamma_{opt,QPHD}$
a	0.305	$0.215 - j0.217$	$-0.321 + j0.259$
b	32.043	$17.888 + j26.586$	$0.087 + j0.109$
c	10.796	$7.907 - j7.351$	$0.596 - j0.254$
d	11.101	$2.787 - j10.745$	$0.117 - j0.363$

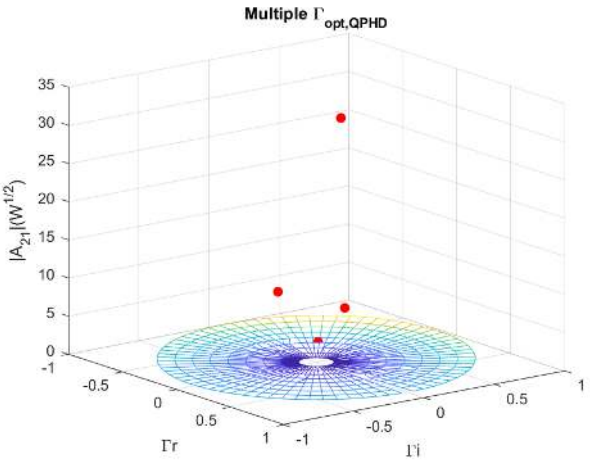

FIGURE 5. QPHD models multiple predictions for optimum loads represented in 3D. The three points above the surface are invalid solutions to the large-signal matching problem.

'a' in Table 1). Hence only this value can be considered to accurately reflect real-world behaviour. In essence, all other values are extrapolations. This is particularly problematic for the QPHD model, since the predicted scattered wave B_{21} value grows without bound as the square of the incident wave A_{21}.

Hence, the first entry in Table 1 (i.e. $\Gamma_{\mathrm{L}} = -0.321 + j0.259$) is the only value that can be 'trusted' to give a realistic optimum load reflection coefficient for maximum output power. Indeed, this value is closest to the actual optimum load point as revealed by measurements – see Fig. 7.

In Fig. 5 it is shown how all bar one of the predicted optimum A_{21} values are high above the mesh of measured values i.e., most predicted optimum loads have very large $|A_{21}|$ values, well beyond the measured range. This means that even though these A_{21} values achieve a realistic A_{21}/B_{21} ratio resulting in a Γ_{L} value that is inside the Smith chart, the A_{21} and B_{21} values that lead to these reflection coefficients are derived from extrapolated values of A_{21} that poorly model the real system. The advantage of the Padé-based model is that in the vast majority of cases it produces no erroneous solutions since (when used with equal order numerator and denominator expansions) it remains bounded for extreme values of A_{21}.

B. QPHD AND PADÉ MODEL COMPARISON FOR MAXIMUM OUTPUT POWER

Fig. 6 shows the real-world measured optimum load, as determined through brute force loadpull measurements on the real device. Also on this figure are the two predicted optimum loads for maximum output power, one from the QPHD

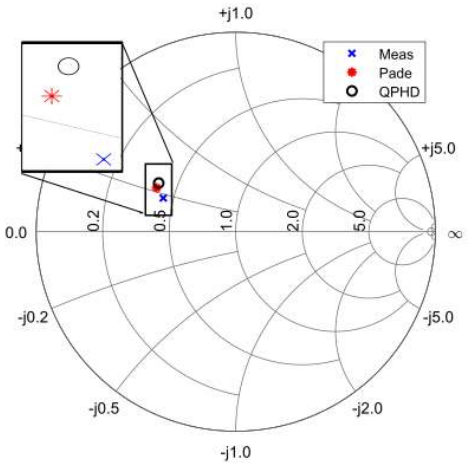

FIGURE 6. Models predictions of optimum loads for maximum power delivered at 20 dBm input power represented on a Smith chart.

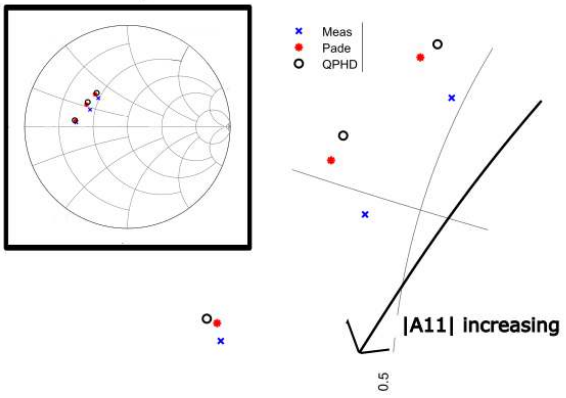

FIGURE 7. Smith chart representing optimum loads (measured and modelled) for maximum output power, corresponding to input powers of 10 dBm, 20 dBm and 30 dBm.

model, and one from the Padé-based model. Both models are extracted from the same data, using the load pattern shown in Fig. 2. In both cases, the models are based on a 50 Ω large-signal operating point, with the model attempting to account for the deviations away from this point.

Another advantage of the Padé-based model may also be observed in Fig. 6: the optimum load predicted from the Padé-based model is closer to the measured (i.e. true) optimum than that predicted by the QPHD model. While this variation appears minor on the plot, it can be significant when trying to achieve the best possible output power from a PA, for example. In Fig. 7, the measured versus modelled optimum load across a range of input power levels can be observed. Shown are both the Pade-based [11/11] model and the QPHD model. It is shown that Padé-based model outperforms the QPHD model across all input powers, as expected.

C. QPHD AND PADÉ MODEL COMPARISON FOR MAXIMUM DRAIN EFFICIENCY

This section demonstrates how the PHD formalism may be used to determine the load impedance required for optimum drain efficiency. Results from the current state-of-the-art

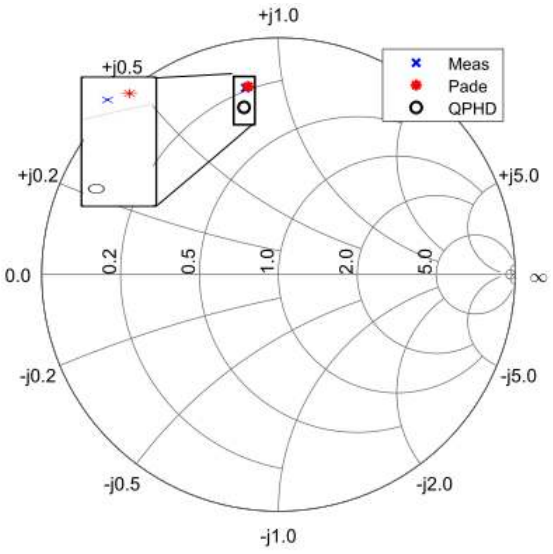

FIGURE 8. Models predictions of optimum loads for maximum drain efficiency represented on a Smith chart.

QPHD model are compared to those obtained from the Padé-based model proposed in this work.

In order to predict drain efficiency, a model for the dc drain current must first be formulated. The dc drain current of the transistor can be modelled in a similar fashion to the X-parameter model (for simplicity – of course a QPHD, or even Padé-based model, could be considered instead for higher accuracy). The dc drain current is the current at port index $i = 2$, and is modelled as follows

$$I_D = X_2^I(|A_{11}|) + \sum_{(i,j)\neq(1,1)} \mathbb{R}\{X_{2,jl}^Y(|A_{11}|.A_{jl}\} \qquad (19)$$

where $\mathbb{R}\{\cdot\}$ denotes the real part.

For a constant dc drain voltage (28 V in this case), the drain efficiency is calculated as

$$\eta_D = \frac{P_{\text{OUT}}}{P_{\text{DC}}} = \frac{|B_{21}|^2 - |A_{21}|^2}{2.V_D.I_D}. \qquad (20)$$

Such a drain current model has been extracted for the same device as used in Sec. III-B. In Fig. 8, a comparison is shown between the Padé [11/11] model prediction and the QPHD model prediction, along with the real-world measured optimum drain efficiency. We clearly see the efficacy of the Padé [11/11] model over the QPHD model, with the former achieving a near perfect prediction, while the QPHD model provides a prediction which is even farther away from the true optimum (blue cross) than we have seen previously with the load predictions from the two models for maximum output power.

Fig. 9 shows a 3D plot of the measured drain efficiency across the full Smith chart, along with the predictions for the QPHD and Padé-based models – this is effectively providing the same basic information as that in Fig. 8, along with information on the rate of change of the efficiency i.e., note the

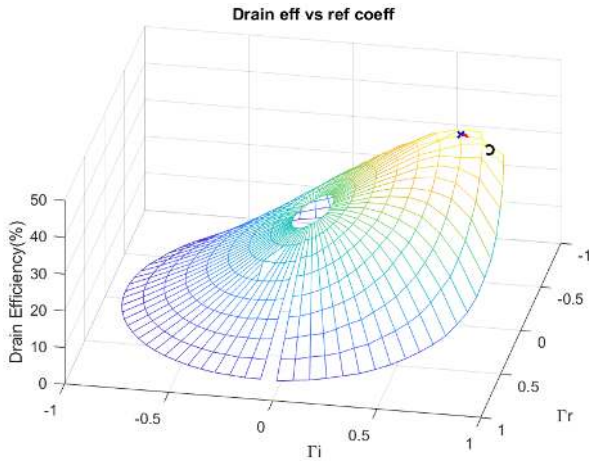

FIGURE 9. Example for determining the optimum load for maximising drain efficiency for a GaN HEMT transistor (P_{IN} = 20 dBm), by comparing results from a Padé 11/11 model and a QPHD model to measurement results.

TABLE 2. Γ_{err} for drain efficiency.

P_{in} (dBm)	$\Gamma_{opt,\,meas}$	$\Gamma_{err,\,QPHD}$	$\Gamma_{err,\,Padé}$
10	$-0.139 + j0.788$	0.0819	0.0135
20	$-0.181 + j0.676$	0.1448	0.0201
30	$-0.354 + j0.354$	0.0941	0.0965

expected steep roll-off in the efficiency around the optimum load, as the load approaches the edge of the Smith chart.

To facilitate a more quantitative comparison, the distance is recorded between the measured optimum load point and the optimum load predicted by the models. The exact equation used is shown below,

$$\Gamma_{err} = |\Gamma_{opt,meas} - \Gamma_{opt,mod}|, \tag{21}$$

where $\Gamma_{opt,meas}$ is the measured reflection coefficient corresponding to maximum drain efficiency, while $\Gamma_{opt,mod}$ is the corresponding prediction from the model.

These load reflection coefficient errors are given in Table 2, for both the QPHD and Padé-based models. Both models show good accuracy, however the the Padé [11/11] model shows consistent higher fidelity across a relatively wide measured power range.

Table 3 shows the efficiency at the two predicted optima from the models, versus input power. As expected, for low input powers the drain efficiency is poor. However, in all cases the measured and modelled efficiencies are remarkably close – a feature of directly-extracted behavioural models.

IV. ADVANCED APPLICATIONS

A. INTELLIGENT LOAD-PULL AND LOAD-DEPENDENT MODELS

The concept of an intelligence-driven load-pull system has been discussed briefly in the literature [23]. Specifically, the main desire is for a load-pull system that can intelligently determine the area(s) of the Smith chart to explore in order to maximise a given metric (e.g. output power)

TABLE 3. Drain efficiency by model predict opt loads.

P_{in} (dBm)	DE % (meas)	DE % (QPHD)	DE % (Padé)
10	15.498	15.326	15.398
20	47.455	44.767	47.070
30	67.617	66.8173	66.756

while minimising the number of measurements, and hence minimise the measurement time.

Alternatively to minimising time, extra measurements could be taken in the vicinity of the optimum Smith chart area of interest, in order to extract a highly accurate *load-dependent* model. Pichler *et al.* [12] shows that load-dependant X-parameter models can achieve superior results compared with regular X-parameters which are extracted under nearly-matched conditions. It seems pertinent therefore to investigate whether higher order PHD models, such as the Padé [11/11] model and the QPHD model, can themselves be extended to load-dependent models for further prediction accuracy. This section attempts to answer this question, while also comparing the efficacy of these higher-order PHD models against each other, in the context of adherence to real-world measured data.

In order to build a load-dependent model, the loadpull system first needs to determine an area of interest on the Smith chart, around which a model can be extracted. Ideally, this would be an area where it is suspected that a certain quantity, say output power, may be maximised. In general, this is not known apriori. In this work, we overcome this problem through the use of a simple X-parameter-based model which may be extracted around the matched condition (usually 50 Ω) and solved, analytically, as in [22], to obtain a rough estimate of where to center the load-dependent model. This can be done very quickly, and automatically, by the loadpull system, and tends to yield reasonably accurate estimates [12]. It is important to realise that this initial X-parameter-based estimate need not be perfect; it need only be accurate enough in order to form the center a load-dependent extraction grid, subsequent measurements will collect enough data to correct small to moderate errors.

For an input power of 10 dBm, the load-dependent model center (aka, the LSOP) is taken to be equal to the predicted load for maximum output power from an X-parameter model exacted at 50 Ω. Load points are then selected around this initial LSOP in order to extract load-dependant higher order models. Fig. 10 shows the load-center (red circle), as well points around this LSOP from which the extraction of load-dependent QPHD and Padé-based models will take place (blue crosses).

Fig. 11 compares the predicted optimum load impedance for maximising output power from both QPHD and Padé-based load-dependent models. It is clear that the load-dependent Padé [11/11] model has a more accurate prediction than previously when extracted around the 50 ohm load point in Section III-B. It is also seen that the Padé-derived prediction is significantly more accurate than that from the QPHD load-dependant model. Indeed,

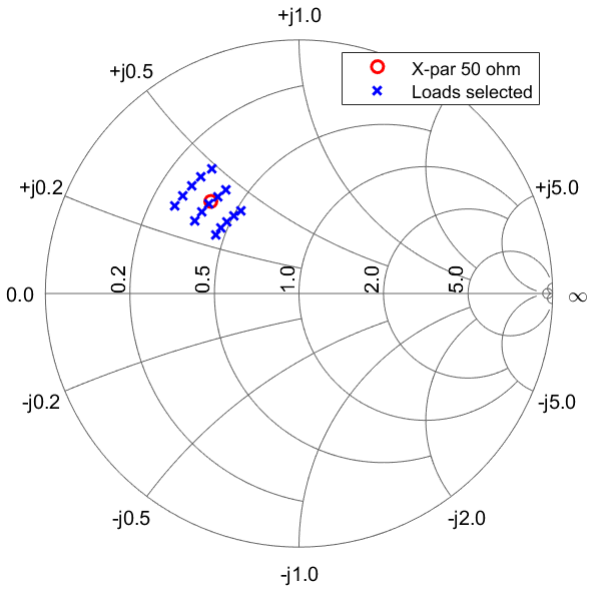

FIGURE 10. Sample of load points taken for model extraction for load-dependant models.

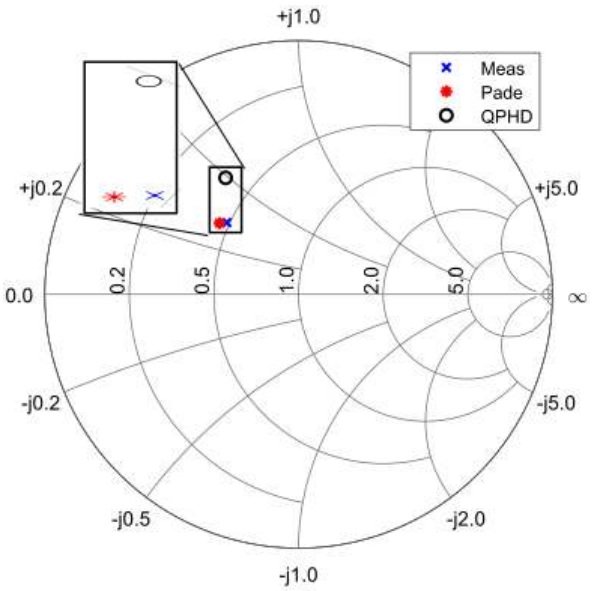

FIGURE 11. Results for load-dependant models.

it is interesting to note that the QPHD model actually yields poorer results than previously when extracted around the 50 ohm load point. A possible explanation for this lies in the symmetric nature of the quadratic curve; it is ideally suited to modelling data that are symmetric as is typically the case with output power or efficiency data centred on 50 Ω; the quantity is maximised inside the Smith chart disk ($\Gamma_L < 1$) and reaches a minimum at the edge ($\Gamma_L = 1$) where the output power is zero. When the model center is moved closer to the Smith chart edge, a quadratic curve is less suitable. Hence, for this reason, the Padé-based model in this work represents the only higher order general load-dependent model proven to work correctly.

In terms of numerical values the maximum power delivered at the LSOP given in Fig. 11 is 26.79 dBm. The Padé model predicted optimum load value would deliver a power of 26.77 dBm while QPHD optimum load value would only deliver a power of 26.57 dBm.

B. EXTEND TO 2-PORT MODEL

Until now, all published PHD-based models concerned with analytic/numerical determination of maximum output power and/or efficiency are solely based on one-port device descriptions i.e. the focus is typically only on port-two, as that is the port with the load that is being varied. However, for certain metrics of interest, such as operating gain, defined as

$$G_p = \frac{P_{out}}{P_{in}} \tag{22}$$

it is necessary to consider both ports.

This above situation would appear to complicate matters, since it is now required to obtain the optimal values of both port-one and port-two variables to, say, maximise the operating gain. However, if we consider an input-matched device, the scattered wave at port-one can be described in terms of the LSOP due to the input and output scattered waves, plus some variation due to the mismatch at port-2, i.e.

$$B_{11} = F_{11}(A_{11}, A_{21}) + X^S_{21,11}A_{21} + X^T_{21,11}A^*_{21}, \tag{23}$$

since for matched input conditions A_{11} is constant. Essentially, all travelling waves in the model are then expressed in terms of A_{21}, with A_{11} being a constant. This means that for metrics where the value of B_{11} is needed to solve for an optimum load, such as operating gain, the problems reduces to a similar situation to that solved previously i.e., by optimising to a value of A_{21} which gives the maximum of the required metric. To do this, (23) is used along with a value of A_{11} which is constant for a given input power to find the input power as follows

$$P_{in} = \frac{|A_{11}|^2 - |B_{11}|^2}{2} \tag{24}$$

The operating gain can then be simply found by substituting (24) and (10) into (22) and then solving for the values of A_{21} when (22) is stationary, in the same manner as have been used to solve for maximisation of the previous metrics such as power delivered and drain efficiency. Fig. 12 shows the predictions for the optimum load for maximum operating gain for the Padé and QPHD model. Due to the increased complexity of this problem (modelling two ports as opposed to one) there is a slightly more inaccurate solution than what we have seen before for other metrics. Nevertheless, the Padé-based model remains more accurate than the other solutions, and has the added benefit of extensibility, which is problematic in the other models due to numerical/false optima issues.

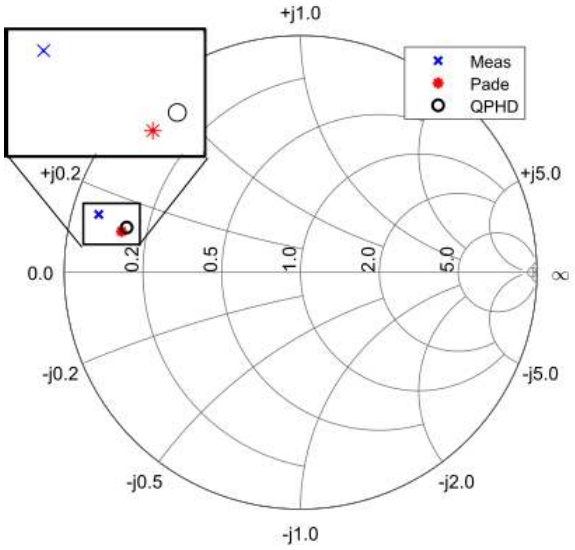

FIGURE 12. **Results for predicting the optimum load point for maximum operating gain. Input power 30 dBm.**

V. CONCLUSION

In this paper, a thorough comparison is presented comparing behavioural device models for a GaN device under large-signal excitation. It is shown that using a Padé approximant-based model, instead of a QPHD model, can increase model accuracy significantly. Several large-signal matching problems (i.e. determination of required load impedance for optimising a given metric) are solved using the Padé and the QPHD models directly, considering maximum power delivered but also, optimising for maximum drain efficiency and maximum operating gain. It is shown that the Padé 11/11 model outperforms the QPHD model when predicting the required load impedances for both power delivered and, separately, drain efficiency. It is also shown how the Padé model does not suffer from the problem of multiple 'false' load optima that the QPHD model is prone to, and furthermore, a method to find the ''valid'' optimum load in the case of multiple solutions, by ruling out invalid solution on the basis of their A_{21} values, is also presented.

REFERENCES

[1] *GSMA: The Mobile Economy*. Accessed: Jan. 25, 2021. [Online]. Available: https://www.gsma.com/mobileeconomy/

[2] M. Meneghini, G. Meneghesso, and E. Zanoni, *Power GaN Devices: Materials, Applications and Reliability*. Cham, Switzerland: Springer, Jan. 2017.

[3] U. K. Mishra, P. Parikh, and Y.-F. Wu, ''AlGaN/GaN HEMTs–An overview of device operation and applications,'' *Proc. IEEE*, vol. 90, no. 6, pp. 1022–1031, Jun. 2002.

[4] E. Aggrawal, K. Rawat, and P. Roblin, ''Investigating continuous class-F power amplifier using nonlinear embedding model,'' *IEEE Microw. Wireless Compon. Lett.*, vol. 27, no. 6, pp. 593–595, Jun. 2017.

[5] M. Koh, J. J. Bell, D. Williams, A. Patterson, J. Lees, D. E. Root, and P. J. Tasker, ''Frequency scalable large signal transistor behavioral model based on admittance domain formulation,'' in *IEEE MTT-S Int. Microw. Symp. Dig.*, Jun. 2014, pp. 1–3.

[6] G. Crupi and D. M. M.-P. Schreurs, *Microwave de-Embedding: From Theory to Applications*. Amsterdam, The Netherlands: Elsevier, 2013.

[7] R. Essaadali, A. Jarndal, A. B. Kouki, and F. M. Ghannouchi, ''A new GaN HEMT equivalent circuit modeling technique based on X-Parameters,'' *IEEE Trans. Microw. Theory Techn.*, vol. 64, no. 9, pp. 2758–2777, Sep. 2016.

[8] G. Gonzalez, *Microwave Transistor Amplifiers: Analysis and Design*. Upper Saddle River, NJ, USA: Prentice-Hall, 1997.

[9] J. Verspecht, D. F. Williams, D. Schreurs, K. A. Remley, and M. D. McKinley, ''Linearization of large-signal scattering functions,'' *IEEE Trans. Microw. Theory Techn.*, vol. 53, no. 4, pp. 1369–1376, Apr. 2005.

[10] Verspecht and D. E. Root, ''Polyharmonic distortion modeling,'' *IEEE Microw. Mag.*, vol. 7, no. 3, pp. 44–57, Jun. 2006.

[11] B. Pichler, G. Magerl, and H. Arthaber, ''A robust extraction technique for second order PHD based behavioral models,'' in *Proc. Int. Workshop Integr. Nonlinear Microw. Millimetre-Wave Circuits (INMMIC)*, Jul. 2018, pp. 1–3.

[12] B. Pichler, G. Magerl, and H. Arthaber, ''A study on quadratic PHD models for large signal applications,'' *IEEE Trans. Microw. Theory Techn.*, vol. 67, no. 7, pp. 2514–2520, Jul. 2019.

[13] G. Baker and P. Graves-Morris, Eds., *Pade Approximants. I. Basic Theory*. Boston, MA, USA: Addison-Wesley, Jan. 1981.

[14] D. E. Root, J. Verspecht, J. Horn, and M. Marcu, *X-Parameters: Characterization, Modeling, and Design of Nonlinear RF and Microwave Components* (The Cambridge RF and Microwave Engineering Series). Cambridge, U.K.: Cambridge Univ. Press, 2013.

[15] S. J. Gillespie, D. E. Root, M. Marcu, and P. H. Aaen, ''Electrothermal X-Parameters for dynamic modeling of RF and microwave power transistors,'' in *Proc. 13th Eur. Microw. Integr. Circuits Conf. (EuMIC)*, Sep. 2018, pp. 353–356.

[16] G. Simpson, J. Horn, D. Gunyan, and D. E. Root, ''Load-pull + NVNA = enhanced X-parameters for PA designs with high mismatch and technology-independent large-signal device models,'' in *Proc. 72nd ARFTG Microw. Meas. Symp.*, Dec. 2008, pp. 88–91.

[17] J. Verspecht, D. Gunyan, J. Horn, J. Xu, A. Cognata, and D. E. Root, ''Multi-tone, multi-port, and dynamic memory enhancements to PHD nonlinear behavioral models from large-signal measurements and simulations,'' in *IEEE MTT-S Int. Microw. Symp. Dig.*, Jun. 2007, pp. 969–972.

[18] J. Cai, J. B. King, B. M. Merrick, and T. J. Brazil, ''Padé-approximation-based behavioral modeling,'' *IEEE Trans. Microw. Theory Techn.*, vol. 61, no. 12, pp. 4418–4427, Dec. 2013.

[19] J. Cai, J. B. King, A. Zhu, J. C. Pedro, and T. J. Brazil, ''Nonlinear behavioral modeling dependent on load reflection coefficient magnitude,'' *IEEE Trans. Microw. Theory Techn.*, vol. 63, no. 5, pp. 1518–1529, May 2015.

[20] J. Cai and T. J. Brazil, ''Reduced-complexity polynomial based nonlinear behavioral modeling,'' *IEEE Microw. Wireless Compon. Lett.*, vol. 24, no. 7, pp. 496–498, Jul. 2014.

[21] R. H. Jones and G. J. Makinson, ''The generation of chisholm rational polynomial approximants to power series in two variables,'' *IMA J. Appl. Math.*, vol. 13, no. 3, pp. 299–310, Jun. 1974, doi: 10.1093/imamat/13.3.299.

[22] D. E. Root, J. Verspecht, and J. Xu, ''Closed-form solutions to large-signal PA problems: Wirtinger calculus applied to X-parameter,'' in *Proc. 12th Eur. Microw. Integr. Circuits Conf. (EuMIC)*, Oct. 2017, pp. 212–215.

[23] T. Williams, B. Wee, R. Saini, S. Mathias, and M. V. Bossche, ''A digital, PXI-based active load-pull tuner to maximize throughput of a load-pull test bench,'' in *Proc. 83rd ARFTG Microw. Meas. Conf.*, Jun. 2014, pp. 1–4.

CIARÁN WILSON (Member, IEEE) received the B.Sc. and M.E. degrees in electronic and computer engineering from University College Dublin (UCD), Dublin, Ireland, in 2015 and 2016, respectively, where he is currently pursuing the Ph.D. degree with the RF and Microwave Research Group.

His research interest includes nonlinear electrothermal device modeling for high-power gallium nitrite (GaN) devices.

ANDING ZHU (Senior Member, IEEE) received the Ph.D. degree in electronic engineering from University College Dublin (UCD), Dublin, Ireland, in 2004.

He is currently a Professor with the School of Electrical and Electronic Engineering, UCD. He has published more than 130 peer-reviewed journal articles and conference papers. His research interests include high-frequency nonlinear system modeling and device characterization techniques, high-efficiency power amplifier design, wireless transmitter architectures, digital signal processing, and nonlinear system identification algorithms.

Dr. Zhu is also an elected member of the MTT-S Administrative Committee (AdCom). He was the General Chair of the 2018 IEEE MTT-S International Microwave Workshop Series on 5G Hardware and System Technologies (IMWS-5G). He is also the Chair of the Electronic Information Committee and the MTT-S Microwave High-Power Techniques Committee and the Vice-Chair of the Publications Committee. He has served as the Secretary for MTT-S AdCom in 2018. He was a Guest Editor of the IEEE TRANSACTIONS ON MICROWAVE THEORY AND TECHNIQUES on 5G Hardware and System Technologies. He is also an Associate Editor of the IEEE Microwave Magazine and a Track Editor of the IEEE TRANSACTIONS ON MICROWAVE THEORY AND TECHNIQUES.

JIALIN CAI (Senior Member, IEEE) received the B.E. degree in electronic engineering from Zhejiang University, Hangzhou, China, in 2007, the M.E. degree from Southeast University, in 2010, respectively, and the Ph.D. degree in electronic engineering from University College Dublin, Dublin, Ireland, in 2015.

From 2015 to 2016, he was a Postdoctoral Researcher with the University of Aveiro, Aveiro, Portugal. He is currently an Associate Professor with the Key Laboratory of RF Circuit and System, Ministry of Education, Hangzhou Dianzi University, Hangzhou, China. His main research interests include active device, circuit and system-level modeling, and the analysis and design of nonlinear microwave circuits, in particular, the RF power amplifiers.

JUSTIN B. KING (Senior Member, IEEE) received the B.E. degree in electronic engineering from University College Dublin (UCD), Dublin, Ireland, and the Ph.D. degree in transistor device modeling from the RF and Microwave Research Group, UCD, in 2012, under the supervision of Prof. Thomas Brazil.

He joined the School of Electrical and Electronic Engineering, UCD, as an Academic Staff, in 2014. He is currently an Assistant Professor with Trinity College Dublin, Ireland. His current research interests include nonlinear electrothermal device characterization, with emphasis on high-power GaN transistor modeling for modern PA design, and device physics, nonlinear circuit simulation algorithms, and modeling for antenna arrays. He is also a member of the MTT-S Young Professionals Committee. He has served on the TPC for both national and international conferences.